IOPscience iopscience.iop.org

Home Search Collections Journals About Contact us My IOPscience

An *ab initio* study of singlet and triplet Rydberg states of N_2

This article has been downloaded from IOPscience. Please scroll down to see the full text article.

2013 J. Phys. B: At. Mol. Opt. Phys. 46 145102

(http://iopscience.iop.org/0953-4075/46/14/145102)

View the table of contents for this issue, or go to the journal homepage for more

Download details:
IP Address: 2.102.169.7
The article was downloaded on 03/07/2013 at 23:28

Please note that terms and conditions apply.

J. Phys. B: At. Mol. Opt. Phys. **46** (2013) 145102 (14pp) doi:10.1088/0953-4075/46/14/145102

An *ab initio* study of singlet and triplet Rydberg states of N_2

Duncan A Little and Jonathan Tennyson

Department of Physics and Astronomy, University College London, Gower Street, London WC1E 6BT, UK

E-mail: duncan.little.11@ucl.ac.uk

Received 28 March 2013
Published 26 June 2013
Online at stacks.iop.org/JPhysB/46/145102

Abstract

Potential energy curves for electronically excited states of molecular nitrogen are calculated using three different *ab initio* procedures. The most comprehensive of these involves the use of scattering calculations, performed at negative energy using the UK molecular *R*-matrix method. Such calculations are used to characterize all the Rydberg states of N_2 with $n \leqslant 6$ and $\ell \leqslant 4$ as well as many higher states including some Rydberg states associated with the first excited A $^2\Pi_u$ state of N_2^+. Many of these states are previously unknown. The calculations are performed at a dense grid of internuclear separations allowing the many avoided crossings present in the system to be mapped out in detail. Extensive comparisons are made with the previously available data for excited states of N_2.

S Online supplementary data available from stacks.iop.org/JPhysB/46/145102/mmedia

(Some figures may appear in colour only in the online journal)

1. Introduction

Nitrogen molecule, N_2, is a strongly bound diatomic system which makes up the majority of the Earth's atmosphere. Other than studies of states of $^1\Sigma_u^+$ and $^1\Pi_u$ symmetry, the literature on electronic excited states is surprisingly brief. Few experimental studies have probed the Rydberg series of triplet and gerade symmetry that underlie the first ionization limit with a similar paucity of theoretical treatments.

Lofthus and Krupenie (1977) gave a comprehensive summary of the observed electronic spectra of N_2 considering the lowest 15 or so electronic states, later updated by Huber and Herzberg (1979). Since, there have been numerous experimental studies (Suzuki and Kakimoto 1982, Roncin *et al* 1984, Verma and Jois 1984, Roncin *et al* 1989, Stahel *et al* 1983, Huber and Jungen 1990, Roncin *et al* 1991, Levelt and Ubachs 1992, Edwards *et al* 1993, van der Kamp *et al* 1994, Whang *et al* 1996, Kawamoto *et al* 1997, Roncin *et al* 1998, de Lange and Ubachs 1999, Sprengers *et al* 2004, Cossart and Cossart-Magos 2004, Hashimoto and Kanamori 2006, Lewis *et al* 2008a, 2008b). All but a few of these studies are measurements of transitions involving the $^1\Sigma_u^+$ and $^1\Pi_u$ states. More recently, Hashimoto and Kanamori (2006), Lewis *et al* (2008b) and Lewis *et al* (2008a) have measured the $^3\Sigma_u^+$ and $^3\Pi_u$ states. Cossart and Cossart-Magos (2004) measured the d_3 $^1\Sigma_g^+$ state for the first time. There have been a number of theoretical calculations, most notably (Ermler *et al* 1982, Spelsberg and Meyer 2001, Michels 2007, Ndome *et al* 2008, Hochlaf *et al* 2010a, 2010b). Studies attempting to model the Rydberg states or Rydberg components of states are isolated to Spelsberg and Meyer (2001) and Hochlaf *et al* (2010b). Spelsberg and Meyer (2001) give a particularly detailed *ab initio* study of the interaction between N_2 Rydberg and valence states, albeit only for two symmetries. We make comparisons with this work below. Finally, we note that Guberman (2007) and Guberman (2012) presented curves for studies of the dissociative recombination (DR) of the N_2^+ ion. The interaction of these curves with bound Rydberg states of the system are important for DR studies and provided the impetus for our calculation of the Rydberg states.

This paper presents a comprehensive set of curves for the singlet and triplet Rydberg states of N_2; states up to g-wave character are considered. Three different *ab initio* procedures are employed in the study. However, our final results were obtained by finding bound states with a scattering calculation. *R*-matrix based scattering calculations have been used to give excellent results for the electronic states of HeH (Sarpal *et al* 1991), which are all of Rydberg character.

 © 2013 IOP Publishing Ltd Printed in the UK & the USA

Corresponding calculations on the electronic states of NO (Rabadán and Tennyson 1996, 1997) and CO (Chakrabarti and Tennyson 2006) showed that whilst this method can provide comprehensive data on Rydberg states, it is not the method of choice for characterizing the low-lying valence states of the system. This issue will be discussed further below.

2. Method

2.1. R-matrix method

Bound state calculations were performed using the *R*-matrix method as implemented in the UKRMol code suite (Carr *et al* 2012). This is an *ab initio*, time-independent variational method which combines quantum chemistry methods with scattering theory to model electron–molecule collisions. The molecular *R*-matrix method and UKRMol codes have been described extensively elsewhere (Gillan *et al* 1995, Tennyson 2010, Carr *et al* 2012), thus only a brief description highlighting the parts relevant to this calculation is given here. The defining feature of the *R*-matrix method is the partitioning of space into two distinct regions by a sphere of radius a, here taken to be 10 a_0, centred on the centre-of-mass of the molecule. This sphere separates the 'inner region' from the 'outer region', which is the space outside of the sphere. Within the inner region, the scattering electron is considered to be indistinguishable from the electrons of the target molecule, hence correlation and exchange effects must be taken into consideration. Beyond a, in the outer region, the electron is treated as being distinct and only long range interactions are considered. The inner region is split again into two separate calculations; a target calculation, which just considers the N target electrons interacting, and a target plus electron or $N + 1$ calculation, in which the scattering electron is allowed to interact with all target electrons in the active space. The results of these two calculations are then combined in the outer region to calculate scattering properties. A balanced treatment between these two calculations is crucial for obtaining good results (Tennyson 1996b). The *R*-matrix itself is the interface between the two separate regions and constructed on the boundary between them; it acts to link the inner region solutions to their matching asymptotic scattering solution.

For bound state solutions, the inner region wavefunction is given by

$$\Psi_n = \sum_k A_k(E_n)\psi_k^{(N+1)} \tag{1}$$

where E_n is the energy of the bound state and $\psi_k^{(N+1)}$ are given by the standard close-coupling expression:

$$\Psi_k^{N+1}(x_1, \ldots, x_{N+1}) = \mathcal{A}\sum_{ij} a_{ijk}\phi_i^N(x_1, \ldots, x_N)u_{ij}(x_{N+1}) + \sum_i b_{ik}\chi_i^{N+1}(x_1, \ldots, x_{N+1}), \tag{2}$$

where ϕ_i^N is the N-electron target wave functions of the ith state and u_{ij} is an orbital used to represent the jth continuum electron with a partial wave expansion up to some maximum value of ℓ, $\ell_{\max}$; the subscript k denotes the kth inner region wave function; $\mathcal{A}$ is an antisymmetrization operator introduced so that the indistinguishable inner region electrons satisfy the Pauli principle; a_{ijk} and b_{ik} are the coefficients of expansions. χ_i are multi-centred, square-integrable functions which are zero on the *R*-matrix boundary and are hence known as the L^2 configurations. The L^2 configurations allow for the relaxation of the orthogonalization between the target and continuum states of the same symmetry and in this work are made up of the target occupied and virtual orbitals. In principle *R*-matrix construction requires all the solutions of the inner region problem. For larger models this becomes computationally impractical and in these cases a partitioned *R*-matrix procedure (Tennyson 2004), was used in which only the 3000 lowest solutions were explicitly considered.

2.2. Target calculation

Rydberg states of N_2 can be represented as an electron interacting with the appropriate state of the 'target' N_2^+ ion. A number of N_2^+ target models were tested. The recipe given below is for our final, or 'best model'; alternative models are introduced, as needed, to assess the stability of our results. Multi-configuration self-consistent field (MCSCF) molecular orbitals (MOs) averaged over the first four states were generated using quantum chemistry code MOLPRO (Werner *et al* 2010) and the Gaussian type orbital (GTO) cc-pVQZ basis of Dunning with a complete active space (CAS) of nine electrons distributed between three σ_g, three σ_u, one π_u and one π_g orbitals with four electrons frozen in the first two σ orbitals. This CAS can be denoted $(1\sigma_g, 1\sigma_u)^4(2\sigma_g, 3\sigma_g, 2\sigma_u, 3\sigma_u, 1\pi_u, 1\pi_g)^9$. Note that since both MOLPRO and the GTO 'polyatomic' implementation of the UK molecular *R*-matrix codes (Morgan *et al* 1998) use only Abelian symmetries, all calculations reported here were actually performed using D_{2h} symmetry. In most cases it is straightforward to transform these results to the higher linear-molecule, $D_{\infty h}$ symmetry and $D_{\infty h}$ symmetry designations are used below for all cases where these can be assigned unambiguously.

All 110 MOs generated in the MOLPRO calculation were then reordered and renormalized to be used with the UKRMol code suite. The target state wavefunctions are then calculated using a configuration–interaction (CI) expansion of individual N electron configurations using the CI program SCATCI (Tennyson 1996a). For balance and consistency the same CAS was used for the target state CI calculation as the MOLPRO calculation. Eight target states were calculated for each of the 16 symmetries (singlet and triplets in D_{2h} representation) resulting in 128 target states. This was then reduced to the lowest 100 for the $N + 1$ calculation to ensure the following, firstly, that no state is generated in D_{2h} symmetry without its $D_{\infty h}$ degenerate pair, for example an A_g state and a B_{1g} state are needed to form a Δ_g state. Secondly, the effects of the inevitable switching of states in energy order with changing internuclear separation are minimized by using a large number of states. Despite taking these measures, there are still minor discontinuities in a small number of curves, the most significant in the G $^3\Delta_g$ state ($\sim$ 0.04 eV) at 1.614 Å.

2.3. $N + 1$ electron inner region calculation

The $(N + 1)$-electron calculation is essentially an extension of the target calculation in which the scattering electron is introduced into the CI. To accommodate the scattering electron continuum orbitals must be included in the calculation. These continuum orbitals take the form of bond-centred GTOs fitted to Bessel functions for $\ell \leqslant 4$ (Faure *et al* 2002). Although it would be expected that GTOs fitted to Coulomb functions would give better results for an ionic target, this was not found to be the case; the completeness of the cc-pVQZ basis resulted in some linear dependence between target and continuum orbitals when the Coulomb functions were used. The MOs calculated for the target were also used in the $N + 1$ calculation. The continuum orbitals are Schmidt orthogonalized to the target MOs and then just the continuum orbitals are symmetric-orthogonalized so all orbitals are orthonormal. Due to the numerical nature of the orthogonalization procedure, orbital combinations which are effectively linearly dependent have small but not precisely zero eigenvalues of the overlap matrix. Therefore a deletion threshold is set below which all eigenvalues are assumed to represent linearly dependent combinations which can safely be removed from the basis. In this work this threshold was set at the default value of 10^{-7}. The raw boundary amplitudes of the orthogonal continuum orbitals needed to construct the R-matrix are also computed at this point. The CAS for the $N + 1$ electron calculation was augmented with 14 virtual orbitals to $(5\sigma_g, 5\sigma_u, 3\pi_u, 2\pi_g, 1\delta_u, 1\delta_g)$ which are important for modelling the valence character of the electronic states (see below). Here the term 'virtual orbitals' is taken to mean the target orbitals not occupied in the N or $N + 1$ CAS. Extra configurations of this form were added to the L^2 functions, the second term in equation (2). This formulation can be described as using 'uncontracted' virtual orbitals, as 'contracted' virtual orbitals are included in the continuum functions; for a discussion on this issue see Tennyson (1996b) and Dora *et al* (2009). Thus, the L^2 functions employed take two different forms: those in which the scattering electron enters the target active space, relaxing the orthogonality between the target and continuum orbitals, such configurations can be represented as $(1\sigma_g, 1\sigma_u)^4(2\sigma_g, 3\sigma_g, 2\sigma_u, 3\sigma_u, 1\pi_u, 1\pi_g)^{10}$, and those in which the scattering electron occupies the virtual orbitals given by $(1\sigma_g, 1\sigma_u)^4(2\sigma_g, 3\sigma_g, 2\sigma_u, 3\sigma_u, 1\pi_u, 1\pi_g)^9(4\sigma_g, 5\sigma_g, 4\sigma_u, 5\sigma_u, 2\pi_u, 3\pi_u, 2\pi_g, 1\delta_u, 1\delta_g)^1$. Calculations were performed for all 16 symmetries at 0.001 Å intervals to give smooth curves which do not need to be fitted.

This study aims to characterize as many of the electronically bound singlet and triplet states of molecular nitrogen as possible. Three different methods of doing so were explored. Firstly, standard electronic structure calculations using models such as multi-reference CI (MRCI) were performed using MOLPRO. These calculations struggle to reproduce the same number of Rydberg states found in the R-matrix bound states, but are generally more accurate for states with a strong valence character. Secondly, the calculations exploited the facility present in the R-matrix codes to search for negative energy, or bound, 'scattering' states. Thirdly, it is possible to use the R-matrix codes to find bound state wavefunctions directly with the form of equation (2), as opposed to equation (1). These two possibilities are discussed, in turn, below. As our continuum basis spans only orbitals up to g-wave, this study will be limited to Rydberg states with $\ell \leqslant 4$. This is not a severe restriction as one can expect states with $\ell \geqslant 5$ to have quantum defects which are very close to zero.

2.4. Outer region bound state calculations

After solving for the inner region wavefunctions the target properties, the $(N + 1)$-eigenpairs and raw boundary amplitudes are combined in an interface program, to produce the information necessary to compute the R-matrix on the boundary. At this point all but the first five (four in $D_{\infty h}$) target states ($^2\Sigma_g^+$, $^2\Pi_u$, $^2\Sigma_u^+$ and $^4\Sigma_u^+$ at equilibrium) are dispensed with. This increases the speed of the outer region calculation tenfold, and leads to greater numerical stability as the channels associated with the highly excited target states are strongly closed. The R-matrix is then built on the boundary and the wavefunction integrated to a distance of 30.1 a_0 from where an asymptotic Gailitis expansion is used. The bound state energies were calculated by using the method described by Sarpal *et al* (1991). This method, an implementation of that by Seaton (1985), centres around finding the roots of an energy dependent determinant $B(E)$; these roots can be found by searching a nonlinear grid of quantum defects, as described by Rabadán and Tennyson (1996). The values of quantum defect are generally concentrated around zero thus a finer grid is used near to integer values of effective quantum number ensuring that no bound states are missed. Modifications were made to the procedure of Rabadán and Tennyson (1996) so that it no longer ignores low-lying valence states which do not have Rydberg-like quantum defect characteristics. Finally we note that despite the use on an improved Runge–Kunta–Nystrom integration procedure (Baker *et al* 1999), as implemented by Zhang *et al* (2011), the bound state routine still gave a considerable number of false detections. These were easily removed as they did not form curves.

2.5. Quantum chemistry-style calculations

Another option within the UKRMol code suite is to completely ignore the outer region and treat the $N+1$-electron calculation as a standard bound state electronic structure calculation. This is achieved by not correcting the integrals for the GTO tails (Morgan *et al* 1997), which go beyond the inner region boundary, allowing the target plus continuum orbital set to span an extended region. These calculations were performed for the same number of symmetries and internuclear separations as the full, bound state R-matrix calculation described above as a means of comparison, an example of this can be seen in figure 2.

3. Initial calculations

3.1. Target tests

A correct representation of the target ion is essential to accurately represent Rydberg states. Target state curves were

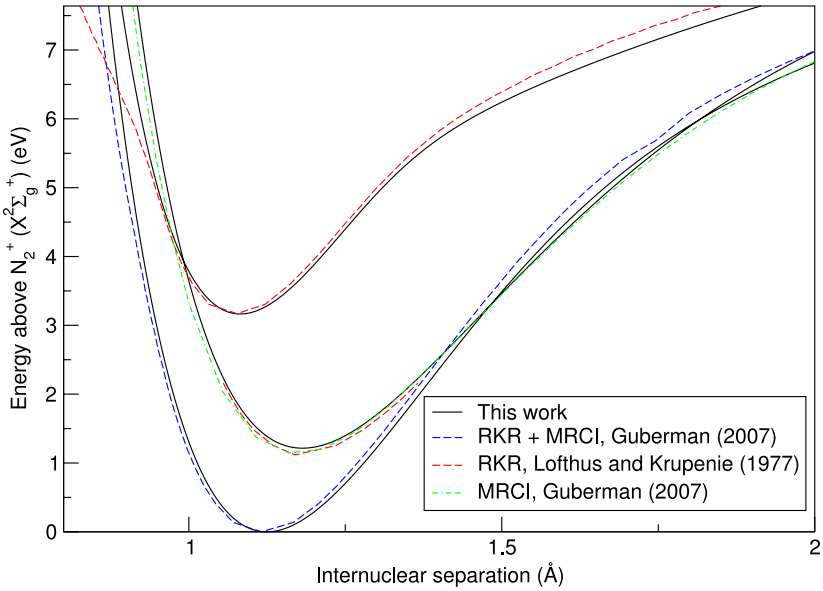

Figure 1. Potential energy curves of the ground state and first two excited states of N_2^+ used as the representation of the target. A comparison is given with empirical RKR curves given by Lofthus and Krupenie (1977) and those extended and calculated by Guberman (2007).

Table 1. Vertical equilibrium excitation energies (eV) and equilibrium positions (Å) for the ground state and first two excited states of the ionic target.

	This work		Experiment[a]		Comparison	
State	T_e	R_e	T_e	R_e	ΔT_e[b]	ΔR_e[b]
$X\,^2\Sigma_g^+$	0.0	1.125	–	1.116 42	–	−0.008 58
$A\,^2\Pi_u$	1.215	1.181	1.1365	1.174 9	−0.0785	−0.006 1
$B\,^2\Sigma_u^+$	3.165	1.082	3.1568	1.074	−0.0082	−0.008 0

[a] Huber and Herzberg (1979).
[b] Obs.—Calc.

calculated using ccp-VDZ, ccp-VTZ and ccp-VQZ bases. The agreement with the experimental curves given in Lofthus and Krupenie (1977) when using the ccp-VQZ basis was good enough that further tests seemed superfluous (see figure 1). In any case going beyond ccp-VQZ with the *R*-matrix method can lead to issues resulting from the target basis functions being too diffuse and crossing the inner region boundary. The agreement between the vertical excitation energies of the target model for the first two excited states ($^2\Pi_u$ and $^2\Sigma_u^+$) at equilibrium internuclear separation is very good (see table 1). The general agreement of the potential energy curves for these three states with the RKR curves given by Lofthus and Krupenie (1977) and extended by Guberman (2012) is good, see figure 1.

3.2. $N + 1$ *electron tests*

As the *R*-matrix method involves combining two different variational electronic structure calculations, the target and $N+1$ electron, there is always an issue of balance between the two calculations. 'Improving' the $N + 1$ electron calculation results in the lowering of energies of *R*-matrix poles and henceforth increases the binding energies of bound states, potentially moving resonant scattering states to bound states. Conversely, lowering the target state energies results in *R*-matrix poles moving up in energy relative to the ground state of the target. Therefore, correctly balancing a model is integral to its development and reliability when using the *R*-matrix method. For a more detailed discussion on balance see Tennyson (2010).

Initial tests involved contracted virtual orbitals with an $N + 1$ CAS of $5\sigma_g$, $3\sigma_u$, $2\pi_u$ and $1\pi_g$ orbitals. Calculations showed that this was unbalanced with respect to the target and the valence states were too high in energy. We then uncontracted the virtual orbitals and extended the CAS to sensible sizes dictated by the MCSCF calculation. We found that going beyond the number of virtual orbitals included in the L^2 functions reported in section 2.3, resulted in an unbalanced calculation, giving an ionization energy that was much too high. With a view to improving the overall balance, the target CAS was expanded; however, this merely made the calculation intractably large and slow for very little gain in accuracy. Efforts were made throughout the model development process to keep the calculation times short, without diminishing the accuracy, meaning that many internuclear separations could be calculated in a reasonable time.

An attempt was made to increase the size of the target calculation without significantly increasing the size of the $N + 1$ calculation. The target calculation was extended to allow a single electron only to occupy the $4\sigma_g$, $4\sigma_u$ and $2\pi_g$ orbitals; this can be thought of as having the original target CAS described in section 2.2, with an additional $(1\sigma_g, 1\sigma_u)^4(2\sigma_g, 3\sigma_g, 2\sigma_u, 3\sigma_u, 1\pi_u, 1\pi_g)^8(4\sigma_g, 4\sigma_u, 2\pi_g)^1$. This gave less accurate results, largely due to the difficulties in finding a CAS for the MCSCF calculation that was consistent with the target calculation and also converged. Rotating orbitals after the MCSCF calculation was also explored in an attempt to better represent the valence states, these rotations

severely disrupted the representation of the target states. As the main aim of the study was to calculate Rydberg states this approach was abandoned.

Beyond the smaller basis sets described in section 3.1 the more diffuse basis set aug-ccp-VQZ was tested; this led to significant linear dependence errors in the orbital orthogonalization step and we concluded the ccp-VQZ basis was sufficiently diffuse, and complete for an accurate description of the Rydberg states. Natural orbitals (NOs) calculated using an MRCI were also tested as an alternative to MCSCF orbitals. The NOs gave very similar results to the MCSCF orbitals and their generation slowed the calculation significantly so were not used. Other tests involving the orbitals used included adding more states to the MOLPRO calculation with different weightings and averaging across the orbitals of two separate N_2^+ and N_2 MCSCF calculations. The former made little difference to energies as long as sensible weightings were used, and the latter again disrupted the target.

Attempts were made to follow the recipe provided by Spelsberg and Meyer (2001) for the b′ $^1\Sigma_u^+$, c′$_4$ $^1\Sigma_u^+$, c′$_5$ $^1\Sigma_u^+$, b $^1\Pi_u$, c$_3$ $^1\Pi_u$ and o$_3$ $^1\Pi_u$ states. This involved performing repeated MCSCF calculations for the orbital generation in which the CAS was built up in each repetition with single occupancy orbital occupation restrictions being applied. Higher energy orbitals beyond the CAS were also rotated down, for example, the first pair of δ_g orbitals. Although we could correctly generate the orbitals in MOLPRO to repeat the essentials of the MRCI calculation given by Spelsberg and Meyers, implementing these orbitals within the *R*-matrix calculation in a meaningful and consistent way proved difficult. Firstly, these orbitals were generated for N_2 and not N_2^+ meaning that the target calculation suffered; it proved difficult to include the orbitals generated using the Spelsberg and Meyer (2001) recipe in a MCSCF N_2^+ calculation which would converge. Secondly, central to Spelsberg and Meyer's method is the inclusion of diffuse bond-centred s and p orbitals, and an augmented basis set; these types of orbitals are not usually included in an *R*-matrix calculation until the $N + 1$ stage; and as mentioned above the use of the aug-ccp-QVZ created linear dependence problems. Lastly, Spelsberg and Meyer's calculation was a specific attempt to calculate three states for two different symmetries, hence could afford to tailor the orbitals to optimize the representation of particular states. As we are attempting to create a model which will give reasonable results for all symmetries we do not have that option. As a result it is not expected to produce valence state curves on a similar scale of accuracy to Spelsberg and Meyer (2001).

It should be noted that although we endeavoured to produce valence states as accurately as possible, the ionization energy of our final model is 0.407 eV too high. This leads to poorly represented equilibrium energies when compared with experimental data or MRCI calculations. This problem can be attributed to the top down approach of the *R*-matrix bound state calculation method we have used, the calculation accuracy decreases with energy relative to the ion ground state. Low-lying valence states are best represented using standard quantum chemistry methods such as MRCI. However, these methods struggle to represent genuine Rydberg states.

4. Results

4.1. Ionic target calculation

In table 1 vertical equilibrium excitation energies and equilibrium positions are presented for the ground state and first two excited states of the N_2^+ target calculation; a comparison with experimental values is given. The agreement with experimental data is very good. Potential energy curves for the target can be seen in figure 1, where a comparison is made with the RKR curves given in Lofthus and Krupenie (1977) as well as those which were then extended and supplemented with MRCI curves by Guberman (2007). The agreement is good in the region around equilibrium for all three states and a divergence is only seen at longer bond lengths. The irregularity of the B state RKR potential is explained by an interaction with the C $^2\Sigma_u^+$ state not shown on the figure (Singh and Rai 1966).

For a scattering calculation of the type presented here, it is expected that for only a limited number of target states that is, one or two, will the energies and wavefunctions approach anything like the exact solution of the problem. Therefore, if this is the case, the C state in our calculation is not close enough in energy for this irregularity to be reproduced. However from the point of view of characterizing the bound Rydberg states of the system, this representation of the target should be more than adequate.

4.2. Bound states

Bound state calculations were performed for singlet and triplets for all D_{2h} symmetries. Given the constraint that $\ell \leqslant 4$, this gives $D_{\infty h}$ states of $\Sigma_{g/u}^{+/-}$, $\Pi_{u/g}$, $\Delta_{g/u}$, $\Phi_{u/g}$, Γ_g symmetries. Calculations were performed at a dense grid of 1199 points in the range 0.8 Å$\leqslant R \leqslant$ 1.999 Å, where *R* is the internuclear separation. Use of this grid removed any need to fit the curves. Our raw data for the scattering calculations in each of the D_{2h} symmetries are given in the supplementary material, available from stacks.iop.org/JPhysB/46/145102/mmedia.

Figure 2 compares the ^1A_g data set of scattering bound states with a quantum chemistry-style $N + 1$ calculation as described in section 2.5. For the lower-lying states the two methods give near-identical results. However it is apparent that only the scattering calculations characterize the high-lying Rydberg states. The states predicted by the quantum chemistry calculations which lie above the N_2^+ ion ground state curve cannot be regarded as reliable (Stibbe and Tennyson 1999). At low energies however, for valence type states, the quantum chemistry-style calculation gives very similar, within 0.02 eV, energies to the scattering calculation.

A convenient way of matching the raw data points to make up the potential energy curves is to use quantum defects, in this study defined by

$$E^B(R) - E^T(R) = -\frac{Z^2}{2\nu^2(R)} = -\frac{Z^2}{2(n-\alpha(R))^2} \qquad (3)$$

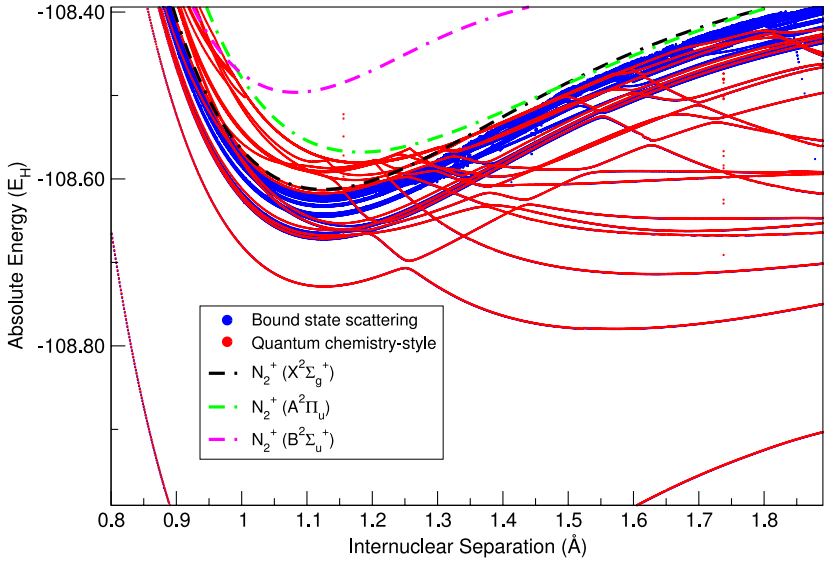

Figure 2. Comparison of a bound state scattering calculation with a quantum chemistry-style calculation as described in the text for ^1A_g symmetry. As this is a calculation in the lower symmetry group D_{2h}, states with symmetries $^1\Sigma_g^+$, $^1\Delta_g$ and $^1\Gamma_g$ all appear on this plot. Spurious data points have been removed. Note that for the lower-lying states the scattering and quantum chemistry-style results coincide.

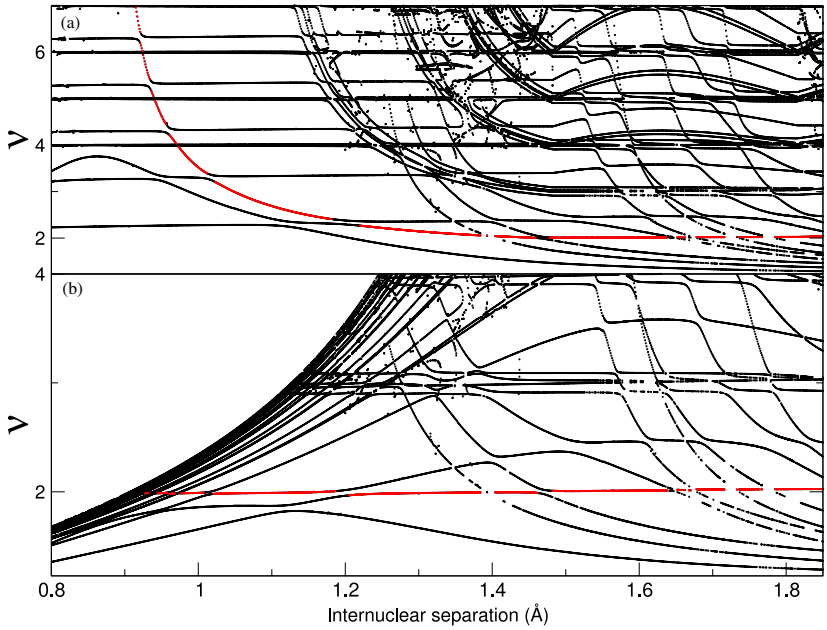

Figure 3. Edlén plots for $^1B_{2u}$ symmetry: (a) effective quantum numbers calculated relative to the ground state, X $^1\Sigma_g^+$; (b) relative to the first excited state A $^2\Pi_u$. Effective quantum numbers of Rydberg states are nearly constant with R if calculated relative to the state they are converging upon and so appear as straight lines on the plot. The red curve illustrates the behaviour of the A $^2\Pi_u(3s\sigma_g)$ state in the two cases.

with energies in Hartrees. E^B is the bound state energy, E^T is the energy of the target state of the ion on which the Rydberg series is converging and Z is the charge of the ionic core, so equals one here. n is the principal quantum number, ν the effective quantum number and α the quantum defect of the Rydberg electron. Quantum defects account for the unshielded Coulombic and non-Coulombic interaction an electron in a Rydberg state will experience when close to the nuclei and inner shell electrons of its parent molecule.

Quantum defects associated with Rydberg states are linear, smooth functions of R when calculated relative to the state on which the Rydberg state is converging, see Rabadán and Tennyson (1997). Plotting ν against R gives what is known as an Edlén plot (Edlén 1964), see figure 3, and provides a useful tool for matching the states when they become close in energy. Two examples are given in the figure, in (a) ν has been calculated relative to the ion ground state and (b) to the first excited state. In (a) the Rydberg states associated with the A state appear as what are known as 'intruder states' passing through the linear states associated with the ground state; whereas in (b) the opposite is true and these states now appear to be linear, an example of this has been highlighted in the figure.

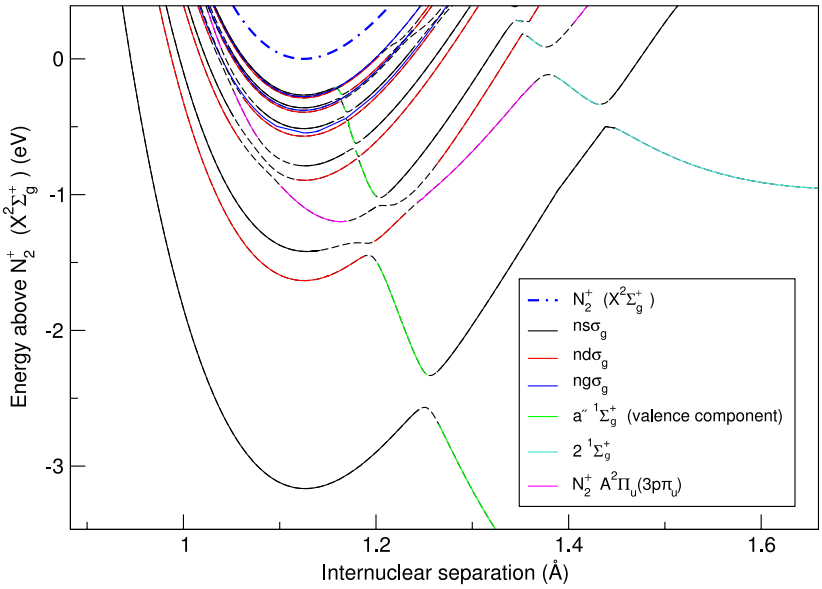

Figure 4. Calculated potential energy curves for the $^1\Sigma_g^+$ symmetry. Coloured are the Rydberg series $ns\sigma_g$, $nd\sigma_g$ and $ng\sigma_g$ as well as $A\,^2\Pi_u(3p\pi_u)$ and valence states $a''\,^1\Sigma_g^+$ and $2\,^1\Sigma_g^+$. The lowest state in the $nd\sigma_g$ series is that assigned by Cossart and Cossart-Magos (2004) to be $d_3\,^1\Sigma_g^+$.

All states were matched by quantum defect without a fitting function. Particularly for weakly bound states, there are a complicated mix of avoided and unavoided crossings brought about respectively by the mix of higher symmetries in the $D_{\infty h}$ being contained within the D_{2h} outputs and valence states passing through the Rydberg series. The numerical instability of the bound state searching algorithm described in section 2.4 leads to two minor issues. Firstly, occasionally the algorithm misses points, leading to gaps in the curves; however, if the missed bond lengths are of particular interest the possibility of fitting the curve still remains. Secondly, the data becomes increasingly noisy at low binding energies and longer bond lengths, or when there are several states interacting. This problem is exacerbated by the proximity of the A state to the ground state which cross at around 1.4 Å. The result of this is that valence, ground state Rydberg states and A state Rydberg states are all present making it difficult to extract meaningful data at energies close to, or above, the equilibrium energy of the ion ground state. We recommend that data above the line of reliability formed by ($R = 1.355$ Å, $E_e = 1.639$ eV) and ($R = 1.905$ Å, $E_e = 6.778$ eV) be treated with caution.

To aid the use of our data we have systematically identified curves matching their quantum defects and total symmetry. Although every effort was made to match the curves as consistently as possible with regards to symmetry, occasionally an avoided crossing appears as a crossing or vice versa. This occurs at points where many curves are interacting and is attributed to numerical noise; in some cases avoided crossings are so narrow they are ignored. A full set of these curves are given in the supplementary data, available from stacks.iop.org/JPhysB/46/145102/mmedia. A typical example of a matched set of curves is given in figure 4 for $^1\Sigma_g^+$ total symmetry. The figure highlights the complexity of the avoided crossing structure inherent in the system as three different types of states (Rydberg converging on $X\,^1\Sigma_g^+$ and $A\,^2\Pi_u$ respectively and valence) interact close to the ionization threshold.

4.3. Valence states

Due to the complexity of the interaction between the valence states and the Rydberg states at low binding energies $\lesssim$5 eV attempting to separate the behaviour for fitting of spectroscopic constants becomes difficult. Hence, we simply provide the adiabatic curves in the supplementary data, available from stacks.iop.org/JPhysB/46/145102/mmedia. Equilibrium energies (E_e) and positions (R_e) are tabulated in table 2 with a comparison to experimental data and previous theoretical calculations. All energies are given relative to the equilibrium energy of the N_2^+ ground state. Table 2 also gives a comparison with Rydberg states of N_2 that have been previously characterized. Due to the interaction with valence states some of the equilibrium positions of the Rydberg states are strongly perturbed. This contributes to the disparity with spectroscopic values if this coupling was not included when the original spectroscopic constants were fitted to the experimental data. Due to the top down approach of our calculation we have presented the energies as being relative to the ion ground state as this gives the best comparison with experimental data. We define our ionization energy as $T_e(N_2^+\,X) = T_0(N_2^+\,X) - \frac{\omega_e}{2}(N_2^+\,X) + \frac{\omega_e}{2}(N_2\,X) = 15.590\,\text{eV}$, where $T_0(N_2^+\,X)$ has been defined relative to $T_0(N_2\,X)$. The spectroscopic parameters are taken from Lofthus and Krupenie (1977). If only T_0 is available then the energy is given relative to T_0 of N_2^+, as this is only the case for comparisons with Rydberg states, the relative correction to T_e is smaller than the accuracy with which we make the comparison, a note has been given on the table if this is the case. As MRCI calculations are optimized relative to the neutral ground state rather than the ion state, this way of presenting data is less favourable to such calculations.

Table 2. Equilibrium binding energies (eV) and equilibrium positions (Å) for valence states and Rydberg states for which experimental data is available. A comparison with spectroscopic data is given when available, all values are from Huber and Herzberg (1979) unless otherwise specified. A comparison is also given with Hochlaf *et al* (2010b) (in-line entry) and Guberman (2012) (entry below in-line).

	This work		Experiment		Comparison[a]		Other theory		Comparison[b]	
State	E_e	R_e	E_e	R_e	ΔE_e	ΔR_e	E_e	R_e	ΔE_e	ΔR_e
$c'_{11}\ ^1\Sigma_u^+$	−0.1259	1.124	−0.1264[h]		−0.0006					
$c'_{10}\ ^1\Sigma_u^+$	−0.1542	1.124	−0.1541[h]		−0.0001					
$c'_9\ ^1\Sigma_u^+$	−0.198	1.124	−0.193[h]		−0.004					
$c'_8\ ^1\Sigma_u^+$	−0.253	1.124	−0.249[h]		−0.004					
$2\ ^1\Pi_u$	−0.340	1.590								
$3\ ^3\Sigma_g^-$	−0.456	1.518								
$c_6\ ^1\Pi_u$	−0.477	1.125	−0.480[e]		0.003					
$c'_7\ ^1\Sigma_u^+$	−0.480	1.125	−0.470[h]		−0.010					
$c_5\ ^1\Pi_u$	−0.722	1.125	−0.730[e]		0.008					
$c'_6\ ^1\Sigma_u^+$	−0.734	1.124	−0.710[h]		−0.024					
$2\ ^1\Pi_g$	−0.893	1.886								
$2\ ^1\Sigma_g^+$	−0.959	1.700								
$c'_5\ ^1\Sigma_u^+$	−1.241[c]	1.136[c]	−1.217[h]		−0.024					
$c_4\ ^1\Pi_u$	−1.222	1.123	−1.253	1.116	0.031	−0.007				
$2\ ^3\Delta_g$	−1.277	1.736								
							−1.195	1.692	−0.082	−0.044
$y\ ^1\Pi_g$	−1.253[c]	1.175[c]	−1.418	1.177	0.165	0.002				
$^1\Phi_u$	−1.314	1.580								
							−1.629	1.565	0.315	−0.015
$z\ ^1\Delta_g$	−1.331[c]	1.155[c]	−1.278	1.169	−0.053	0.014				
$2\ ^1\Delta_g$	−1.361	1.684								
$2\ ^3\Sigma_g^-$	−1.438	1.729					−1.375	1.821	−0.063	0.092
$k\ ^1\Pi_g$	−1.465	1.128	−1.480	1.109	0.015	−0.019				
$1\ ^1\Delta_g$	−1.504	1.732								
$x\ ^1\Sigma_g^-$	−1.539	1.179	−1.526	1.173	−0.013	−0.006				
$d_3\Sigma_g^+$	−1.633	1.125	−1.699[g]		0.066					
$o_3\ ^1\Pi_u$	−2.182[c]	1.170[c]	−2.464	1.178	0.282	0.008				
$H\ ^3\Phi_u$	−2.358	1.512	−2.483	1.488	0.125	−0.024	−2.210	1.499	−0.148	−0.013
							−2.534	1.506	0.176	−0.006
$c_3\ ^1\Pi_u$	−2.488[c]	1.140[c]	−2.637	1.116	0.149	−0.024				
$F\ ^3\Pi_u$	−2.254	1.168	−2.555[f]	1.176[f]	0.301	0.008				
$c'_4\ ^1\Sigma_u^+$	−2.628	1.127	−2.635[h]		0.007					
$G\ ^3\Pi_u$	−2.660	1.127	−2.696[f]	1.113[f]	0.036	−0.014				
$b'\ ^1\Sigma_u^+$	−2.780	1.463	−2.634	1.444	−0.146	−0.019				
							−2.794	1.499	0.014	0.036
$D\ ^3\Sigma_u^+$	−2.724	1.124	−2.603	1.108	−0.121	−0.016				
$b\ ^1\Pi_u$	−3.200	1.340	−2.984	1.284	−0.216	−0.056				
							−3.158	1.381	−0.042	0.041
$1\ ^1\Gamma_g$	−2.765	1.636					−2.821	1.609	0.046	−0.027
							−3.100[d]	1.600[d]	0.335	−0.036
$a''\ ^1\Sigma_g^+$										
Inner	−3.165	1.128	−3.190	1.122	0.025	−0.006	−3.698	1.114	−0.532	−0.014
Outer	−4.553	1.572					−4.367	1.557	−0.195	−0.015
							−4.570	1.574	0.017	0.002
$1\ ^3\Sigma_g^-$	−3.659	1.631					−3.467	1.619	−0.192	−0.012
$C'\ ^3\Pi_u$	−3.755	1.534	−3.396	1.514	−0.359	−0.020	−3.286	1.527	−0.469	−0.007
							−3.698	1.535	−0.057	0.001
$E\ ^3\Sigma_g^+$	−3.575	1.127	−3.705	1.117	0.130	−0.010	−3.700	1.127	0.125	0.000
$C\ ^3\Pi_u$	−4.703	1.162	−4.539	1.149	−0.164	−0.013	−4.401	1.154	−0.302	−0.008
							−4.583	1.160	−0.120	−0.002
$G\ ^3\Delta_g$	−4.876	1.637	−4.692	1.611	−0.184	−0.026	−4.466	1.618	−0.410	−0.019
							−4.608	1.618	−0.268	−0.019
$w\ ^1\Delta_u$	−6.786	1.282	−6.651	1.268	−0.135	−0.014	−6.47	1.295	−0.308	0.013
							−6.763	1.280	−0.023	−0.002
$a\ ^1\Pi_g$	−7.088	1.235	−7.000	1.220	−0.088	−0.015	−6.915	1.223	−0.173	−0.012
							−7.043	1.226	−0.045	−0.009
$a'\ ^1\Sigma_u^-$	−7.274	1.292	−7.140	1.276	−0.134	−0.016	−7.031	1.278	−0.243	−0.014
$B'\ ^3\Sigma_u^-$	−7.667	1.292	−7.373	1.278	−0.294	−0.014	−7.349	1.283	−0.318	−0.009
$W\ ^3\Delta_u$	−8.499	1.293	−8.175	1.300	−0.324	0.007	−8.147	1.283	−0.352	−0.010
							−8.243	1.285	−0.256	−0.008

Table 2. (Continued.)

	This work		Experiment		Comparison[a]		Other theory		Comparison[b]	
State	E_e	R_e	E_e	R_e	ΔE_e	ΔR_e	E_e	R_e	ΔE_e	ΔR_e
$B\,^3\Pi_g$	−8.494	1.227	−8.198	1.213	−0.296	−0.014	−8.106	1.220	−0.388	−0.007
							−8.242	1.218	−0.252	−0.009
$A\,^3\Sigma_u^+$	−9.946	1.310	−9.366	1.287	−0.580	−0.023	−9.392	1.292	−0.554	−0.018
							−9.460	1.291	−0.486	−0.019
$X\,^1\Sigma_g^+$	−15.997	1.107	−15.590	1.098	−0.407	−0.009	−15.590	1.104	−0.407	−0.003

[a] Obs.—Calc.
[b] Other—This work.
[c] Perturbed equilibrium position.
[d] Michels (2007).
[e] Lofthus and Krupenie (1977), only T_0 available.
[f] Lewis *et al* (2008b).
[g] Cossart and Cossart-Magos (2004), only T_0 available.
[h] Huber and Jungen (1990), only T_0 available.

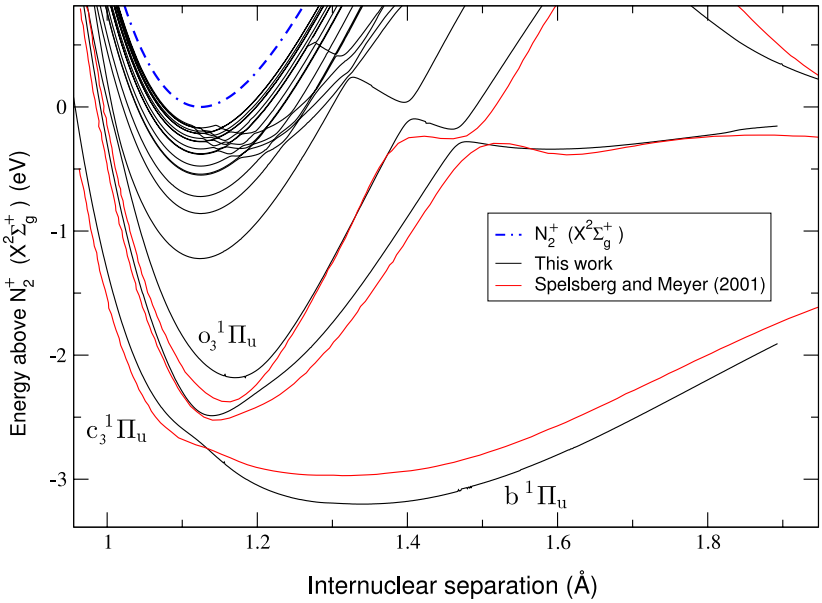

Figure 5. N_2 electronically excited states of $^1\Pi_u$ symmetry compared to those of Spelsberg and Meyer (2001).

The agreement in equilibrium position with experiment is good, all being within 5% of the experimental value and the majority within 1.5%. As mentioned in section 3.2, the ionization energy of our model is too high, resulting in poor comparisons with experimental values for some of the valence states; such states largely lie at low energies. This problem arises as the low-lying states are more sensitive to valence shell correlation effects which are difficult to model in a scattering calculation. Despite this the majority of valence state equilibrium energies are within 5% of their experimental values.

We compare with three theoretical studies of similar sophistication to ours, due to Spelsberg and Meyer (2001), Hochlaf *et al* (2010b) and Guberman (2012) all of whom employed MRCI models. Comparisons with Hochlaf *et al* and Guberman are given in table 2. The agreement between calculated equilibrium positions is reasonable. However, as expected, the agreement with equilibrium energy is less favourable. Comparisons with the previous potential curves are given, figures 5 and 6 for Spelsberg and Meyer (2001), figure 7 for Hochlaf *et al* (2010b) and figure 8 for Guberman (2012) and Hochlaf *et al* (2010b). These figures also act as a comparison for the Rydberg states, where they exist, which will be discussed in the following section.

As Spelsberg and Meyer only report equilibrium energies for diabats, their calculated adiabats are placed at the given equilibrium energy of the lowest diabat in figures 5 and 6. For $^1\Pi_u$ the valence state, $b\,^1\Pi_u$ is poorly described by our model at long bond lengths, this is likely to be due to an under representation of the configuration $(\sigma_g^2, \sigma_u^2)(\sigma_g^3, \sigma_u^2, \pi_u^3, \pi_g^2)$. The $o\,^1\Pi_u$ in our model is ∼0.2 eV too high, a result of the A ion state also being slightly too high. The agreement with the $^1\Sigma_u^+$ is good with a favourable comparison with the general shape of the valence state curve; the equilibrium energies are slightly too low.

There appears to be no spectroscopic data for the outer well of the $a''\,^1\Sigma_g^+$; our predictions agree very well with the values calculated by Guberman, and are 0.195 eV lower

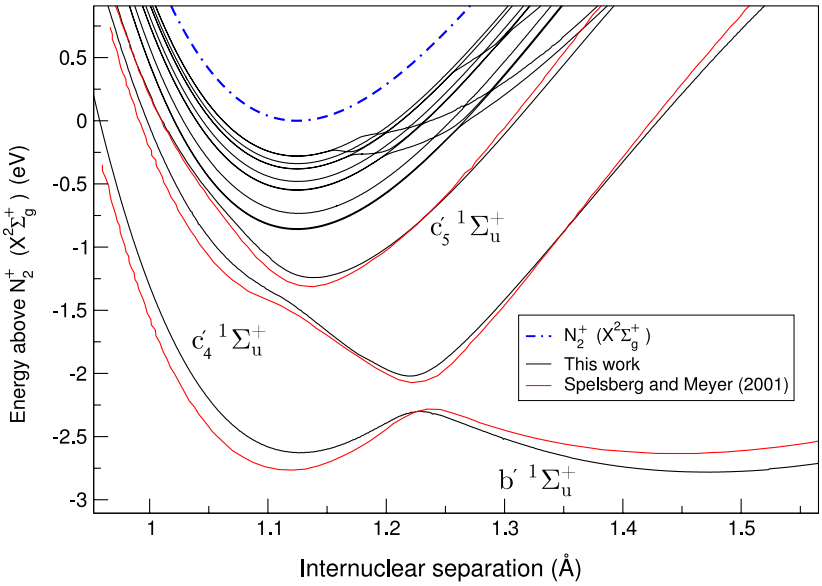

Figure 6. N_2 electronically excited states of $^1\Sigma_u^+$ symmetry compared to those of Spelsberg and Meyer (2001).

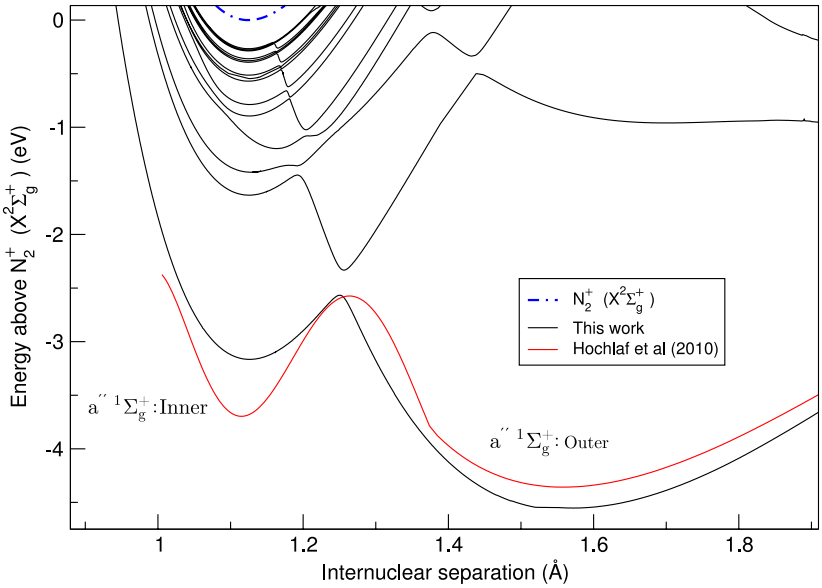

Figure 7. N_2 electronically excited states of $^1\Sigma_g^+$ symmetry compared to Hochlaf *et al* (2010b).

than Hochlaf *et al.* Figure 7 compares our adiabat describing the $^1\Sigma_g^+$ Rydberg and valence states with Hochlaf *et al.* Hochlaf *et al*'s representation of the $a''{}^1\Sigma_g^+$ valence component appears to have a somewhat unphysical shape; furthermore, our Rydberg component traces the shape of the ion ground state curve, as would be expected. This figure again illustrates the suitability of our scattering calculation methodology over MRCI calculations for characterizing Rydberg states.

Figure 8 compares our calculations with Guberman and Hochlaf *et al* for the $^3\Pi_u$ states, important for the DR of N_2^+ (Guberman 2012). The agreement with Guberman is again good, reconfirming the ion crossing point of the $2\,^3\Pi_u$ state. This curve is the major channel in the DR calculation. The curves of Hochlaf *et al* are again higher than both ours and Guberman's.

4.4. Rydberg states

Tables 3–7 give equilibrium positions, energies and quantum defects for Rydberg series converging on the ground state of the ion. Table 8 lists those states which are bound in the N_2 equilibrium region and converge on the excited $A\,^2\Pi_u$ ion state. A note is made if the equilibrium position of the Rydberg state has been perturbed by another Rydberg series or a valence state. A comparison is given with the rather limited data available on quantum defects, with general good agreement. As this is the first comprehensive calculation on Rydberg states of N_2, the comparison with other theoretical data is limited to that already discussed in section 4.3, apart from average quantum defects calculated by Guberman (2012) where the agreement is good. For Rydberg states converging on the ground state

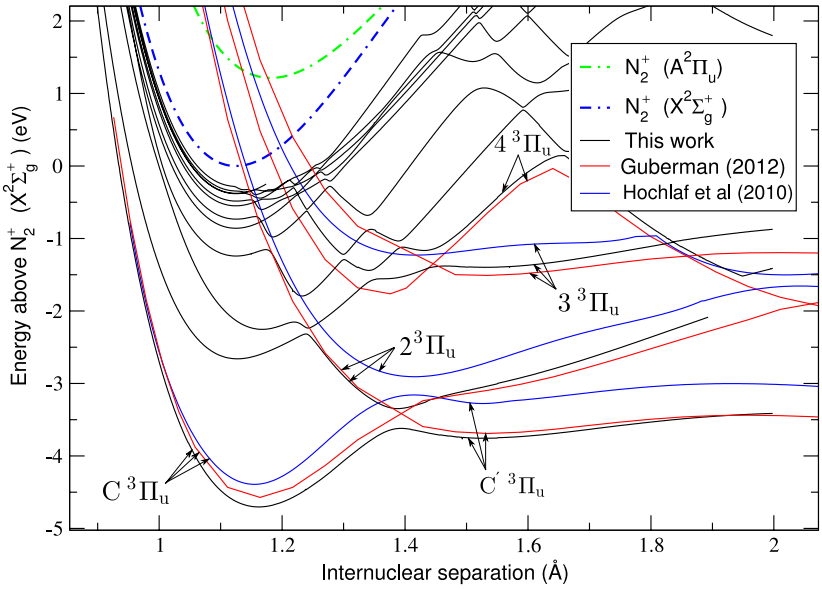

Figure 8. N_2 electronically excited states of $^3\Pi_u$ symmetry compared to those of Hochlaf *et al* (2010b) and Guberman (2012).

Table 3. Equilibrium binding energies (eV), equilibrium positions (Å) and quantum defects for Rydberg states of $^1\Sigma$ and $^1\Pi$ symmetry. Experimental quantum defects are from Lofthus and Krupenie (1977).

	$^1\Sigma_g^+$			$^1\Sigma_u^+$			$^1\Pi_g$			$^1\Pi_u$		
n	E_e	R_e	α	E_e	R_e	α	E_e	R_e	α	E_e	R_e	α
		$s\sigma_g$			$p\sigma_u^b$			$d\pi_g$			$p\pi_u^d$	
3	−3.165[a]	1.128[a]	0.927	−2.628	1.127	0.725	−1.465[c]	1.128[c]	−0.047	−2.488[f]	1.140[f]	0.668[f]
4	−1.419	1.127	0.904	−1.241[f]	1.136[f]	0.700[f]	−0.820	1.125	−0.074	−1.222	1.124	0.663
5	−0.788	1.126	0.844	−0.734	1.124	0.694	−0.528	1.125	−0.078	−0.722	1.125	0.658
6	−0.514	1.125	0.853	−0.480	1.125	0.675	−0.368	1.125	−0.080	−0.477	1.125	0.657
7	−0.360	1.125	0.855	−0.340	1.124	0.670	−0.271	1.125	−0.081	−0.338	1.125	0.659
8	−0.267	1.125	0.857	−0.253	1.124	0.670				−0.254	1.125	0.676
9				−0.198	1.124	0.705						
10				−0.154	1.124	0.608						
11				−0.126	1.124	0.626						
		$d\sigma_g$			$f\sigma_u$			$g\pi_g$			$f\pi_u$	
3	−1.633[e]	1.125[e]	0.114									
4	−0.894	1.126	0.100	−0.861	1.124	0.024				−0.859	1.125	0.020
5	−0.569	1.124	0.112	−0.550	1.124	0.027	−0.546	1.125	0.006	−0.549	1.125	0.022
6	−0.393	1.125	0.116	−0.382	1.124	0.029	−0.379	1.125	0.007	−0.381	1.125	0.025
7	−0.287	1.125	0.119	−0.280	1.125	0.031	−0.278	1.125	0.007	−0.280	1.125	0.034
		$g\sigma_g$										
5	−0.546	1.125	0.007									
6	−0.379	1.125	0.008									
7	−0.278	1.124	0.008									

[a] $a''\,^1\Sigma_g^+$ Inner, Expt. $\alpha = 0.97$.
[b] Series is $c'_{4-11}\,^1\Sigma_u^+$, Expt. $\alpha = 0.608\,22$, (Huber and Jungen 1990).
[c] $k\,^1\Pi_g$.
[d] First four in series are:
$c_3\,^1\Pi_u$, Expt. $\alpha = 0.73$.
$c_4\,^1\Pi_u$, Expt. $\alpha = 0.70$.
$c_5\,^1\Pi_u$, Expt. $\alpha = 0.7$.
$c_6\,^1\Pi_u$, Expt. $\alpha = 0.68$.
[e] $d_3\,^1\Sigma_g^+$, Expt. $\alpha = 0.171$, (Cossart and Cossart-Magos 2004).
[f] Perturbed equilibrium position.

Table 4. Equilibrium binding energies (eV), equilibrium positions (Å) and quantum defects for Rydberg states of $^1\Delta$ and $^1\Phi$ symmetry.

	$^1\Delta_g$			$^1\Delta_u$			$^1\Phi_g$			$^1\Phi_u$		
n	E_e	R_e	α	E_e	R_e	α	E_e	R_e	α	E_e	R_e	α
		$d\delta_g$			$f\delta_u$			$g\phi_g$			$f\phi_u$	
3	−1.539	1.129	0.028									
4	−0.848	1.124	−0.005	−0.861	1.125	0.025				−0.844	1.125	−0.014
5	−0.543	1.125	−0.008	−0.548	1.125	0.018	−0.546	1.125	−0.001	−0.544	1.125	−0.012
6	−0.377	1.125	−0.008	−0.380	1.125	0.016	−0.379	1.125	−0.001	−0.378	1.125	−0.009
7	−0.277	1.125	−0.008	−0.279	1.125	0.017	−0.278	1.125	−0.001	−0.278	1.125	−0.003
8	−0.212	1.125	−0.008	−0.214	1.125	0.021						
9				−0.169	1.125	0.027						
10				−0.137	1.125	0.037						
		$g\delta_g$										
5	−0.546	1.125	0.009									
6	−0.380	1.125	0.014									
7	−0.279	1.125	0.017									
8	−0.214	1.125	0.019									

Table 5. Equilibrium binding energies (eV), equilibrium positions (Å) and quantum defects for Rydberg states of $^3\Sigma$ and $^3\Pi$ symmetry. All experimental quantum defects are from Lofthus and Krupenie (1977).

	$^3\Sigma_g^+$			$^3\Sigma_u^+$			$^3\Pi_g$			$^3\Pi_u$		
n	E_e	R_e	α	E_e	R_e	α	E_e	R_e	α	E_e	R_e	α
		$s\sigma_g$			$p\sigma_u$			$d\pi_g$			$p\pi_u^f$	
3	−3.575[a]	1.127[a]	1.049	−2.724[b]	1.124[b]	0.765	−1.494	1.124	−0.018	−2.660[c]	1.127[c]	0.739[c]
4	−1.680	1.129	1.155	−1.336	1.124	0.809	−0.826	1.126	−0.059	−1.242	1.125	0.690
5	−0.915	1.124	1.143	−0.762	1.125	0.776	−0.532	1.125	−0.055	−0.733	1.123	0.693
6	−0.579	1.124	1.152				−0.371	1.125	−0.053	−0.484	1.126	0.701
7	−0.398	1.125	1.156				−0.274	1.125	−0.051	−0.346[e]	1.125[e]	0.726[e]
		$d\sigma_g$			$f\sigma_u$			$g\pi_g$				$f\pi_u$
3	−1.514	1.128	0.003									
4	−0.840	1.125	0.024	−0.854	1.125	0.008				−0.859	1.125	0.020
5	−0.546	1.125	0.007	−0.547	1.125	0.011	−0.546	1.125	0.006	−0.549	1.125	0.024
6	−0.379	1.124	0.008	−0.380	1.125	0.015	−0.379	1.125	0.007	−0.382[d]	1.125[d]	0.029[d]
7							−0.278	1.125	0.007			
		$g\sigma_g$										
5	−0.539	1.124	−0.023									
6	−0.375	1.124	−0.022									

[a] E $^3\Sigma_g^+$, Expt. $\alpha = 1.08$.
[b] D $^3\Sigma_u^+$, Expt. $\alpha = 0.77$.
[c] G $^3\Pi_u$.
[d] Perturbed equilibrium position.
[e] Series continues but equilibrium positions become ambiguous due to strong perturbations from Rydberg series converging on $A^2\Pi_u$.
[f] Guberman (2012), $R = 1.143$, $\alpha = 0.7540$.

with $n \geqslant 4$ the agreement with spectroscopic data is excellent, in particular the $c'_n\ ^1\Sigma_u^+$ or $^1\Sigma_u^+(ns\sigma_u)$ series. We also confirm the assignment by Cossart and Cossart-Magos (2004) of the $d_3\,^1\Sigma_g^+$ state. For $n = 3$ the agreement is generally good with the highest percentage difference being 5.58% for $c_3\ ^1\Pi_u$. These discrepancies can be accounted for by two factors, a perturbed equilibrium position, the equilibrium position of $c_3\ ^1\Pi_u$ is strongly perturbed and the overestimation of the ionization energy. The comparison with experimental values for Rydberg states converging on the A state is less favourable with a ∼12.5% difference for the $o_3\ ^1\Pi_u$ and $y\ ^1\Pi_g$ states. As indicated earlier this could be partly attributed to the A state being slightly too high in our model and perturbed equilibrium positions.

The agreement with spectroscopic data for the $n \geqslant 4$ states converging on the ground state asserts confidence in the validity of the Rydberg components predicted by this model. The A states should be treated with somewhat more caution, although, with the limited spectroscopic data available it is difficult to make a clear judgement.

Table 6. Equilibrium binding energies (eV), equilibrium positions (Å) and quantum defects for Rydberg states of $^3\Delta$ and $^3\Phi$ symmetry.

	$^3\Delta_g$			$^3\Delta_u$			$^3\Phi_g$			$^3\Phi_u$		
n	E_e	R_e	α	E_e	R_e	α	E_e	R_e	α	E_e	R_e	α
		$d\delta_g$			$f\delta_u$			$g\phi_g$			$f\phi_u$	
3	−1.551	1.131	0.041									
4	−0.850	1.123	0.001	−0.861	1.125	0.026				−0.844	1.125	−0.014
5	−0.547	1.125	0.014	−0.552	1.124	0.033	−0.544	1.124	−0.001	−0.542	1.125	−0.012
6	−0.380	1.125	0.020	−0.380	1.125	0.017	−0.378	1.125	−0.001	−0.377	1.125	−0.008
7				−0.279	1.125	0.019	−0.278	1.125	−0.001			
8				−0.214	1.125	0.025						
9				−0.169	1.125	0.037						
10				−0.138[a]	1.125[a]	0.069[a]						
		$g\delta_g$										
5	−0.545	1.125	0.004									
6	−0.378	1.125	0.004									

[a]Estimated, due to perturbation from Rydberg states converging on $A^2\Pi_u$.

Table 7. Equilibrium binding energies (eV), equilibrium positions (Å) and quantum defects for Rydberg states of Γ symmetry.

	$^1\Gamma_g$			$^3\Gamma_g$		
n	E_e	R_e	α	E_e	R_e	α
		$g\gamma_g$				
5	−0.545	1.125	0.004	−0.543	1.125	−0.008
6	−0.378	1.125	0.004	−0.377	1.125	−0.008
7	−0.278	1.125	0.004			
8	−0.213	1.125	0.005			

Table 8. Equilibrium binding energies (eV), equilibrium positions (Å) and quantum defects for Rydberg states converging on $A\,^2\Pi_u$. The quantum defect is given relative to the $A^2\Pi_u$ state of N_2^+, the term in the parentheses gives the Rydberg electron symmetry. States given with full spectroscopic notation have been characterized previously and appear also in table 2.

State	E_e	R_e	α
$^1\Sigma_g^+(3p\pi_u)$	−1.199	1.163	0.634
x $^1\Sigma_g^-(3p\pi_u)$	−1.347	1.179	0.696
$^1\Sigma_u^-(3d\pi_g)$	−0.232	1.183	−0.066
y $^1\Pi_g(3p\sigma_u)$	−1.253	1.175	0.652
o $^1\Pi_u(3s\sigma_g)$	−2.182	1.170	0.172
z $^1\Delta_g(3p\pi_u)$	−1.331	1.155	0.704
$^1\Delta_u(3d\pi_g)$	−0.266	1.180	−0.031
$^3\Sigma_g^+(3p\pi_u)$	−1.482	1.189	0.768
$^3\Sigma_g^-(3p\pi_u)$	−1.349	1.181	0.697
$^3\Sigma_u^-(3d\pi_g)$	−0.237	1.183	−0.061
$^3\Pi_g(3p\sigma_u)$	−1.278	1.163	0.672
F $^3\Pi_u(3s\sigma_g)$[a]	−2.254	1.168	1.022
$^3\Delta_g(3p\pi_u)$	−1.486	1.196	0.760
$^3\Delta_u(3d\pi_g)$	−0.296	1.197	0.009

[a] Guberman (2012), $R = 1.164$, $\alpha = 1.009$.

5. Conclusions

We have used a procedure based on finding negative energy scattering states to identify the electronically excited states of the nitrogen molecule. The method is not competitive with high quality *ab initio* calculations for the low-lying valence curves but gives very good results for Rydberg states when, as here, a good representation of the ion is included in the calculation. We used this procedure to systematically characterize the singlet and triplet Rydberg series of N_2, the majority of them for the first time. The use of a computationally rapid procedure means that we have been able to compute the curves on a dense grid of points allowing the complicated nature of the many avoided crossings present in the system to be mapped out in detail and removing the need to fit the underlying curves. The comparison with spectroscopic data where available gave excellent agreement for Rydberg states converging on the ground state with $n \leqslant 4$ and we recommend the use of these curves.

Our aim is to extend these scattering calculations into the continuum to identify those resonance curves which are important for studies of dissociative recombination (DR). The good agreement we have obtained for the key dissociative curves when compared to previous studies suggests that such calculations should be able to provide reliable, *ab initio* curves which can be used as a starting point for the calculation of DR cross sections. This is in contrast to previous studies on similar size molecules where it has proved necessary to adjust the curves to successfully model DR (Schneider *et al* 2000). Furthermore, the detailed characterization of the Rydberg–valence state interactions, and particularly the avoided crossings, should allow the calculation of reliable DR branching ratios; this was recently highlighted as an issue in a review of nitrogen chemistry in Titan's atmosphere (Dutuit *et al* 2013).

Acknowledgment

We thank Professor M Hochlaf for supplying their data and Themisys Limited for supporting a studentship for DAL.

References

Baker T S, Dormand J R and Prince P J 1999 *Appl. Numer. Math.* **29** 171–88

Carr J M, Galiatsatos P G, Gorfinkiel J D, Harvey A G, Lysaght M A, Madden D, Masin Z, Plummer M and Tennyson J 2012 *Eur. J. Phys.* D **66** 58

Chakrabarti K and Tennyson J 2006 *J. Phys. B: At. Mol. Opt. Phys.* **39** 1485–97

Cossart D and Cossart-Magos C 2004 *J. Chem. Phys.* **121** 7148–52

de Lange A and Ubachs W 1999 *Chem. Phys. Lett.* **310** 471–6

Dora A, Bryjko L, van Mourik T and Tennyson J 2009 *J. Chem. Phys.* **130** 164307

Dutuit O *et al* 2013 *Astrophys. J. Suppl.* **204** 20

Edlén B 1964 *Handbuch der Physik* vol 27 (Berlin: Springer)

Edwards S, Roncin J Y, Launay F and Rostas F 1993 *J. Mol. Spectrosc.* **162** 257–67

Ermler W C, McLean A D and Mulliken R S 1982 *J. Phys. Chem.* **86** 1305–14

Faure A, Gorfinkiel J D, Morgan L A and Tennyson J 2002 *Comput. Phys. Commun.* **144** 224–41

Gillan C J, Tennyson J and Burke P G 1995 *Computational Methods for Electron-Molecule Collisions* ed W Huo and F A Gianturco (New York: Plenum) pp 239–54

Guberman S L 2007 *J. Phys. Chem.* A **111** 11254–60

Guberman S L 2012 *J. Chem. Phys.* **137** 074309

Hashimoto T and Kanamori H 2006 *J. Mol. Spectrosc.* **235** 104–10

Hochlaf M, Ndome H and Hammoutène D 2010a *J. Chem. Phys.* **132** 104310

Hochlaf M, Ndome H, Hammoutène D and Vervloet M 2010b *J. Phys. B: At. Mol. Opt. Phys.* **43** 245101

Huber K and Herzberg G 1979 *Constants of Diatomic Molecules* (New York: Van Nostrand-Reinhold)

Huber K P and Jungen C 1990 *J. Chem. Phys.* **92** 850–61

Kawamoto Y, Fujitake M and Ohashi N 1997 *J. Mol. Spectrosc.* **185** 330–5

Levelt P F and Ubachs W 1992 *Chem. Phys.* **163** 263–75

Lewis B R, Baldwin K G H, Heays A N, Gibson S T, Sprengers J P, Ubachs W and Fujitake M 2008a *J. Chem. Phys.* **129** 204303

Lewis B R, Heays A N, Gibson S T, Lefebvre-Brion H and Lefebvre R 2008b *J. Chem. Phys.* **129** 164306

Lofthus A and Krupenie P H 1977 *J. Phys. Chem. Ref. Data* **6** 113–307

Michels H H 2007 *Electronic Structure of Excited States of Selected Atmospheric Systems* (New York: Wiley)

Morgan L A, Gillan C J, Tennyson J and Chen X 1997 *J. Phys. B: At. Mol. Opt. Phys.* **30** 4087–96

Morgan L A, Tennyson J and Gillan C J 1998 *Comput. Phys. Commun.* **114** 120–8

Ndome H, Hochlaf M, Lewis B R, Heays A N, Gibson S T and Lefebvre-Brion H 2008 *J. Chem. Phys.* **129** 164307

Rabadán I and Tennyson J 1996 *J. Phys. B: At. Mol. Opt. Phys.* **29** 3747–61

Rabadán I and Tennyson J 1997 *J. Phys. B: At. Mol. Opt. Phys.* **30** 1975–88

Rabadán I and Tennyson J 1998 *J. Phys. B: At. Mol. Opt. Phys.* **31** 4485–7 (erratum)

Roncin J Y, Launay F and Larzilliere M 1984 *Phys. Rev. Lett.* **53** 159–62

Roncin J Y, Launay F, Subtil J L and Yoshino K 1991 *Planet. Space Sci.* **39** 1301–4

Roncin J Y, Launay F and Yoshino K 1989 *J. Mol. Spectrosc.* **134** 390–4

Roncin J Y, Subtil J L and Launay F 1998 *J. Mol. Spectrosc.* **188** 128–37

Sarpal B K, Branchett S E, Tennyson J and Morgan L A 1991 *J. Phys. B: At. Mol. Opt. Phys.* **24** 3685–99

Schneider I F, Rabadán I, Carata L, Tennyson J, Andersen L H and Suzor-Weiner A 2000 *J. Phys. B: At. Mol. Opt. Phys.* **33** 4849–61

Seaton M J 1985 *J. Phys. B: At. Mol. Opt. Phys.* **18** 2111–31

Singh R B and Rai D 1966 *J. Mol. Spectrosc.* **19** 424–34

Spelsberg D and Meyer W 2001 *J. Chem. Phys.* **115** 6438–49

Sprengers J, Johansson A, L'Huillier A, Wahlstrm C G, Lewis B and Ubachs W 2004 *Chem. Phys. Lett.* **389** 348–51

Stahel D, Leoni M and Dressler K 1983 *J. Chem. Phys.* **79** 2541–58

Stibbe D T and Tennyson J 1999 *Chem. Phys. Lett.* **308** 532–6

Suzuki T and Kakimoto M 1982 *J. Mol. Spectrosc.* **93** 423–32

Tennyson J 1996a *J. Phys. B: At. Mol. Opt. Phys.* **29** 1817–28

Tennyson J 1996b *J. Phys. B: At. Mol. Opt. Phys.* **29** 6185–201

Tennyson J 2004 *J. Phys. B: At. Mol. Opt. Phys.* **37** 1061–71

Tennyson J 2010 *Phys. Rep.* **491** 29–76

van der Kamp A B, Cosby P and van der Zande W J 1994 *Chem. Phys.* **184** 319–33

Verma R D and Jois S S 1984 *J. Phys. B: At. Mol. Opt. Phys.* **17** 3229

Werner H J *et al* 2010 MOLPRO, a package of *ab initio* programs see www.molpro.net/

Whang T J, Zhao G, Stwalley W C and Wuc C 1996 *J. Quant. Spectrosc. Radiat. Transfer* **55** 335–44

Zhang R, Baluja K L, Franz J and Tennyson J 2011 *J. Phys. B: At. Mol. Opt. Phys.* **44** 035203